

# The first orbital solution for the massive colliding-wind binary HD 93162 ( $\equiv$ WR 25) $\star$

R. Gamen<sup>1,\*\*\*</sup>, E. Gosset<sup>2,\*\*\*</sup>, N. Morrell<sup>3,†</sup>, V. Niemela<sup>4,‡</sup>, H. Sana<sup>2,5</sup>, Y. Nazé<sup>2,§</sup>, G. Rauw<sup>2,\*\*\*</sup>, R. Barbá<sup>1,¶</sup>, and  
G. Solivella<sup>4,||</sup>

(Affiliations are given below the references)

Received <date> / accepted <date>

## ABSTRACT

**Context.** Since the discovery, with the EINSTEIN satellite, of strong X-ray emission associated with HD 93162 ( $\equiv$ WR 25), this object has been predicted to be a colliding-wind binary system. However, radial-velocity variations that would prove the suspected binary nature have yet to be found.

**Aims.** We spectroscopically monitored this object to investigate its possible variability to address this discordance.

**Methods.** We compiled the largest available radial-velocity data set for this star to look for variations that might be due to binary motion. We derived radial velocities from spectroscopic data acquired mainly between 1994 and 2006, and searched these radial velocities for periodicities using different numerical methods.

**Results.** For the first time, periodic radial-velocity variations are detected. Our analysis definitively shows that the Wolf-Rayet star WR 25 is an eccentric binary system with a probable period of about 208 days.

**Key words.** stars: binaries: spectroscopic – stars: massive stars – stars: Wolf-Rayet – stars: individual: HD 93162

## 1. Introduction

Massive stars of spectral type O and Wolf-Rayet (WR) are important objects that play a crucial role in the dynamic and chemical evolution of galaxies. They are the major source of ionizing and UV radiation and, through their huge mass-loss rates, they have a strong mechanical impact on their surroundings. Despite their importance, our knowledge of these objects and of their evolution is still fragmentary. The parameters that predominantly determine the evolution of a massive star are its mass (as for any star in the HR diagram) and its mass-loss rate, although rotation could also have an important impact

(Meynet & Maeder, 2005). In this context, massive O+O and WR+O binaries are key objects because their binary nature allows us to determine minimum masses from the radial velocity orbital solution.

It is now well established that strong winds of massive stars in binary systems collide (Stevens et al., 1992) generating hard X-ray emission. For O stars, this comes in addition to a softer component that is intrinsic to individual objects (Berghöfer et al., 1997; Sana et al., 2006). The existence of intrinsic emission for WR stars is still under investigation (Oskinova et al., 2003; Gosset et al., 2005). As for colliding-wind binaries, the observed characteristics of the collision region may contribute to constrain the mass-loss rates and, eventually, the inclination of those systems (by studying the X-ray emission modulation during the orbital cycle). Although colliding-wind binaries are interesting objects, only a handful of them have been studied in detail, which is particularly true for WR+O systems.

The star HD 93162 (WR 25 in van der Hucht, 2001) is a bright ( $V = 8.1$ ) galactic Wolf-Rayet located in the Carina Nebula region. Its binary nature has been a matter of debate for many years. It has been classified as WN7 + O7 by Smith (1968) because the spectrum appears as a superposition of WN-type emission lines and of absorption lines corresponding to an O-type star. The morphology of the blue

Send offprint requests to: R. Gamen, e-mail: rgamen@dfu1s.c1

$\star$  Based on observations collected at the European Southern Observatory (La Silla, Chile), at the Las Campanas Observatory, at the Cerro-Tololo Observatory (Chile) and at the CASLEO (El Leoncito, Argentina).

\*\* Visiting Astronomer, CASLEO, Argentina, and LCO, Chile

\*\*\* Research Associate FNRS (Belgium)

† Visiting Astronomer, CASLEO, Argentina, CTIO and LCO, Chile

‡ Member of Carrera del Investigador, CIC-BA, Argentina. Visiting Astronomer, CASLEO, Argentina, and CTIO, Chile.

§ Postdoctoral Researcher FNRS (Belgium)

¶ Member of Carrera del Investigador, CONICET, Argentina. Visiting Astronomer, CASLEO, Argentina, and LCO, Chile

|| Visiting Astronomer, CASLEO, Argentina

optical spectrum of WR 25 has been further discussed by Walborn (1974). He classified this star as WN6-A (see also Walborn & Fitzpatrick, 2000) and considered that there was not sufficient information to confirm its binary nature, since absorption lines intrinsic to a WN star had been observed in the neighbouring binary HD 92740 $\equiv$ WR 22 (Niemela, 1973). The massive binary status of WR 22 with absorption and emission lines moving in phase has been confirmed by several authors (Niemela, 1973; Conti et al., 1979; Rauw et al., 1996; Schweickhardt et al., 1999). In later classification systems of WR stars (e.g. van der Hucht et al., 1981; Smith et al., 1996), the presence of absorption lines has been noted in different ways, e.g. "+abs" or adding an "a", indicating that absorption lines of unknown origin are observed in the otherwise emission-line spectrum.

Radial velocity studies of WR-type spectra with absorption lines are thus needed to shed light on the origin of these lines. In the case of WR 25, previously reported radial velocity studies have not revealed any orbital motion. From the study of 15 photographic spectra obtained during consecutive nights, Moffat (1978) concluded that WR 25 is probably a single star. Conti et al. (1979) reached a similar conclusion although they noticed a larger scatter in the radial velocities of WR 25 than that observed for other stars in their study (such as HD 93131 $\equiv$ WR 24 and WR 22 besides its orbital motion).

Using EINSTEIN observations, Seward & Chlebowski (1982) found that WR 25 has an abnormally high X-ray flux and, later, Pollock (1991) suggested that this very high X-ray luminosity might be caused by colliding winds in a binary system. More recently, Raassen et al. (2003) analyzed *XMM-Newton* observations and provided further evidence that the X-ray emission could be indicative of a colliding-wind binary (CWB) although its apparent stability has been, on the contrary, taken as an argument against binarity. Pollock & Corcoran (2006) reported significant variability as detected with *XMM-Newton* and discussed the possibility of periodic variations in the X-ray flux.

Drissen et al. (1992) found polarimetric variability in WR 25, as well as a wavelength dependence of its polarization angle. One of the two proposed explanations was that this variability may arise in a long-period binary system. The alternative explanation attributed particular properties to the intervening interstellar medium. In his recent catalog, van der Hucht (2001) classified WR 25 as WN6h+O4f considering that the WR emission lines showed evidence of being diluted, although no radial-velocity variations had ever been detected.

To investigate the binary status of WR 25, the massive star research groups of Liège and La Plata independently collected high-resolution spectra of this star over the past 10 years. The acquisition of high-resolution spectra of WR stars is rather unusual due to the difficulties presented by the comparatively broad emission lines typical of these stars. However, the radial velocities (RVs) measured for each data set showed variations larger than the expected errors. No single periodicity could be found until the data obtained by the two groups were combined. In the following, we show how the analysis of the combined spectroscopic data set enabled us to reveal the binary nature

**Table 1.** Observing runs. The first column gives the month and year of the observations, the second column lists the instrumental combination utilized. The third column gives the number of spectra.

Date	Instr. configuration	n
High-resolution spectra		
Feb-97	Echelle-REOSC, 2.15-m, CASLEO	2
Mar-97	CES+LC, CAT 1.4-m, ESO	4
Feb-98	Echelle-REOSC, 2.15-m, CASLEO	5
Feb-99	Echelle-REOSC, 2.15-m, CASLEO	3
May-01	FEROS, 1.5-m, ESO	4
Mar-02	FEROS, 1.5-m, ESO	4
Mar-02	EMMI-REMD/Ech, NTT, ESO	2
Apr-02	FEROS, 1.5-m, ESO	1
Jan-03	Echelle-REOSC, 2.15-m, CASLEO	4
Mar-03	Echelle-REOSC, 2.15-m, CASLEO	3
Apr-03	Echelle-REOSC, 2.15-m, CASLEO	5
May-03	FEROS, 2.2-m, ESO	3
Dec-03	Echelle-REOSC, 2.15-m, CASLEO	2
May-04	FEROS, 2.2-m, ESO	3
Apr-05	Echelle, 2.5-m, LCO	4
Feb-06	Echelle, 2.5-m, LCO	1
Medium-resolution spectra		
Feb-94	2D-Frutti, 1-m, CTIO	2
Apr-96	B&C, 1.5-m, ESO	2
Feb-02	CSpec, 1.5-m, CTIO	4
Low-resolution spectra		
May-73	Cass, 0.9-m, CTIO	2
Dec-97	B&C, 2.15-m, CASLEO	4
Apr-01	REOSC-DS, 2.15-m, CASLEO	6

of WR 25 and to derive a preliminary orbital solution for this system.

## 2. Observations and data reduction

Our observational data set consists of 50 high-, 8 medium- and 12 low-resolution spectra obtained, from 1994 to 2006 (except for two spectra acquired in 1973), at different observatories and with various instrumental configurations.

Comparison (wavelength calibration) spectra were obtained at the same telescope positions as the stellar spectra immediately after or before the science exposures, except for FEROS which is stable enough that three to four calibrations over the night are sufficient.

The summary of the observations is presented in Table 1 where we give the dates of the run, the instrumentation used, and the number of spectra obtained.

### 2.1. High-resolution spectra (HRS)

Twenty four echelle spectra were obtained with the REOSC Cassegrain spectrograph (on long-term loan from the University of Liège) attached to the 2.15-m reflector at the

Complejo Astronómico El Leoncito (CASLEO<sup>1</sup>), using a Tek 1024 × 1024 pixel CCD as the detector. These spectra cover an approximate wavelength range from 3600 to 6000 Å, with a spectral resolving power of 26000. Typical S/N ratios in the continuum range between 65 and 100.

Four spectra were acquired with the ESO 1.4-m Coudé Auxiliary Telescope feeding the CES spectrograph equipped with the Long Camera and CCD ESO#38, yielding an effective resolving power of 65000, and a wavelength domain between 4035 Å and 4080 Å. Only the blue path was used and the exposure time was between 30 min and one hour, implying spectra with S/N ratios of 100. Normalization to the continuum was performed through the use of a metal-poor star observed under similar conditions to WR 25.

Fifteen spectra covering the whole optical range (3750–9000 Å) were obtained with the Fiber-fed Extended Range Optical Spectrograph (FEROS), an echelle spectrograph mounted at the ESO 1.5-m telescope at La Silla and then transferred to the ESO/MPI 2.2-m telescope in October 2002. The detector was a 2k × 4k EEV CCD with a pixel size of 15 μm × 15 μm. The spectral resolving power of FEROS is 48000. Typical exposure times were between 10 and 20 min according to weather conditions, resulting in typical S/N ratios in the continuum between 150 and 200 at the 1.5-m and around 250 at the 2.2-m.

Two spectra were acquired with EMMI attached to the Nasmyth focus of the NTT telescope. The instrument was used in the echelle spectrographic mode (REMD-echelle) with grating #9 and grism #3, providing a resolving power of 7700 and 18 usable spectral orders, covering the wavelength domain from 4040 Å to 7670 Å. Typical S/N ratios are around 120.

Five spectra were observed with the 2.5-m du Pont telescope at Las Campanas Observatory (LCO), Chile, using the echelle spectrograph which provides simultaneous wavelength coverage from ~ 3700 to 7000 Å at a typical resolving power of ~40000. The detector is a Tek5 2k × 2k CCD with pixel size of 24 μm. We used a 1 × 4 arcsec slit. These spectra have S/N ratios around 100.

## 2.2. Medium-resolution spectra (MRS)

Two medium-resolution spectra (S/N ~ 100) were obtained in 1996 with the ESO 1.5-m telescope equipped with the modified Boller & Chivens spectrograph at La Silla. The configuration utilized is described in Gosset et al. (2001). Four medium-resolution spectra were obtained with the Cassegrain Spectrograph at the CTIO<sup>2</sup> 1.5-m telescope in February 2002. A 600 l/mm grating blazed at 3375 Å in second order, combined with a Loral 1k CCD provided a 2 pixel resolution of 1.5 Å (wavelength range 3270–4180 Å). Two spectra were observed with the Shectman/Heathcote two-dimensional, photon-counting detector (2D-frutti) on the Cassegrain spectrograph at

the CTIO 1-m telescope. The wavelength coverage was from 3800 to 5000 Å at a 3 pixel resolution of 1.5 Å. Typical S/N ratios range between 50 (2D-frutti data) and 250 (CSpec at CTIO). Typical resolving powers for these MRS are in the range 2000–4000.

## 2.3. Low-resolution spectra (LRS)

We have also obtained lower resolution spectra with resolving powers ~ 1000.

Six LRS were acquired at CASLEO with the above-mentioned REOSC spectrograph but in its simple dispersion mode. This configuration provides a sampling of 1.64 Å per pixel, on the Tek 1024 × 1024 CCD.

We also used 4 spectra observed with the Boller & Chivens spectrograph attached to the 2.15-m telescope at CASLEO. A PM 512 × 512 pixel CCD, with pixel size of 20 μm, was used as the detector. The reciprocal dispersion was ~ 2.3 Å pixel<sup>-1</sup>, and the wavelength region observed was about λλ 3800 – 4800 Å. Typical S/N ratios of CASLEO LRS are about 200.

In addition, we used two previously unpublished radial velocity values determined from spectra observed in May 1973 at CTIO with the Cassegrain spectrograph attached to the 0.9-m telescope. These spectra were recorded on photographic plates, have a reciprocal dispersion of 120 Å/mm, and were widened to 1 mm for a better visibility of the spectral lines. The spectrograms were measured for the determination of RVs with a Grant oscilloscope engine. Because the radial velocity values of the N IV λ4058 emission determined from these two spectra were rather more negative than the mean of the other 52 observations, they were deemed suspect and were not included in the radial velocity study published by Conti et al. (1979). We note, however, that the radial velocity of the interstellar Ca II absorptions in the two photographic spectra (−32 km s<sup>-1</sup>) does not deviate much from the values for these lines in our digital spectra (see below).

## 3. The radial velocity analysis

We have determined the radial velocities of WR 25 measuring the position of the N IV λ4058 emission line because this line is narrow and strong enough to minimize measurement errors. In addition, it is expected to be formed relatively deep in the WR wind, and thus to better reflect the true motion of the WR star. We arbitrarily adopted for that line the rest wavelength λ<sub>0</sub>=4057.9 Å as given by Conti et al. (1977). The adopted method consists of fitting Gaussian profiles to the observed line using either MIDAS or IRAF routines. We worked on spectra normalized to the continuum and, to homogenize the RV measurements, we favoured the position as measured on the upper part of the line; this has the advantage of being less dependent on the errors in the definition of the continuum. The RVs of the N IV λ4058 emission line as measured in the spectra of WR 25 are reported in Table 2. These values should be cautiously considered as preliminary because various effects (e.g. intrinsic line-profile variations) could render the measured RVs inaccurate. On a few good spectra, we used other techniques to measure the position of the N IV λ4058 line, e.g. one based on

<sup>1</sup> CASLEO is operated under agreement between CONICET, SECYT, and the National Universities of La Plata, Córdoba and San Juan, Argentina.

<sup>2</sup> CTIO is operated by the AURA Inc. under a cooperative agreement with the National Science Foundation as part of the NOAO.

**Table 2.** Radial velocities (RVs) of the N IV  $\lambda 4058$  emission line measured in the spectra of WR 25. The velocities are expressed in the heliocentric rest frame; time is given in Heliocentric Julian Date.

HJD	RV	Dataset	HJD	RV	Dataset
2,400,000+	km s <sup>-1</sup>		2,400,000+	km s <sup>-1</sup>	
41823.657	-112	LRS	52328.707	-18	MRS
41828.620	-117	LRS	52328.718	-20	MRS
49406.668	-9	MRS	52333.848	-20	MRS
49409.767	-23	MRS	52335.652	-18	HRS
50181.671	-32	MRS	52337.685	-27	HRS
50182.637	-25	MRS	52338.636	-20	HRS
50505.846	-47	HRS	52339.639	-22	HRS
50507.802	-48	HRS	52353.616	-20	HRS
50531.535	-68	HRS	52353.620	-20	HRS
50531.584	-70	HRS	52383.507	-48	HRS
50532.513	-59	HRS	52655.865	-29	HRS
50534.524	-69	HRS	52657.870	-29	HRS
50807.849	-15	LRS	52658.861	-30	HRS
50809.868	-17	LRS	52659.855	-29	HRS
50811.869	-28	LRS	52710.711	-4	HRS
50812.856	-26	LRS	52711.827	-6	HRS
50842.800	-7	HRS	52712.832	-9	HRS
50846.791	-7	HRS	52735.672	-11	HRS
50847.877	-7	HRS	52736.673	-18	HRS
50850.855	-11	HRS	52737.631	-15	HRS
50852.798	-8	HRS	52738.590	-12	HRS
51209.865	-15	HRS	52739.658	-22	HRS
51216.881	-5	HRS	52782.493	-32	HRS
51218.880	-10	HRS	52783.498	-30	HRS
52005.575	-80	LRS	52784.493	-30	HRS
52007.577	-102	LRS	52985.841	-42	HRS
52008.576	-110	LRS	52989.842	-37	HRS
52009.612	-81	LRS	53131.510	-11	HRS
52011.635	-103	LRS	53133.605	-10	HRS
52013.589	-74	LRS	53135.485	-11	HRS
52037.638	-16	HRS	53480.710	-46	HRS
52038.586	-20	HRS	53481.584	-39	HRS
52039.618	-22	HRS	53488.559	-28	HRS
52040.622	-15	HRS	53490.662	-26	HRS
52328.697	-22	MRS	53772.679	-12	HRS

the lower part of the emission profile. The resulting RVs differ from the adopted RVs measured on the basis of the upper part by  $0.06 \text{ \AA}$  or  $4.5 \text{ km s}^{-1}$  at maximum. No systematic shift has been detected. These results give further support to the reported RVs and provide an idea of the error on the measurement.

In Fig. 1, we show two typical line profiles. One was observed on HJD 2 452 383.507 (corresponding to  $\phi = 0.78$ , see below) and exhibits a RV of  $-48 \text{ km s}^{-1}$ . The other, acquired on HJD 2 453 133.605 ( $\phi = 0.39$ ), corresponds to a velocity of  $-10 \text{ km s}^{-1}$ . These spectra are representative of two extreme positions of the line as observed by us at high resolution. The main difference between the two spectra of Fig. 1 is a Doppler shift and line-profile variations, if they exist, are only second order effects. On the other hand, the smallness of the shift compared to the line width explains the difficulty in performing fully accurate measurements through a fit of the entire profile.

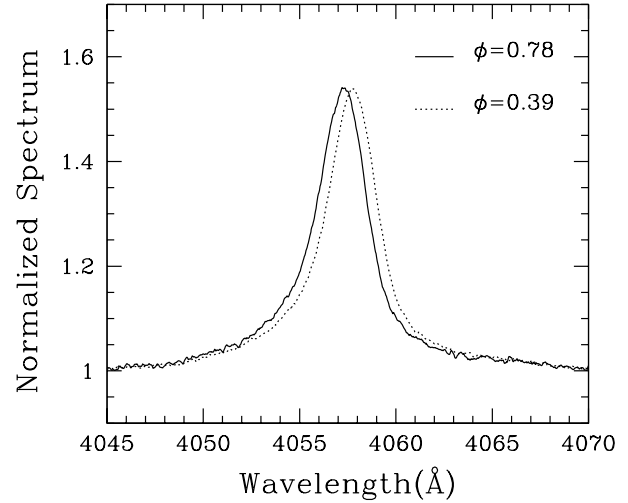


**Fig. 1.** Two typical line profiles corresponding to high S/N FEROS spectra of WR 25. The emission line is N IV  $\lambda 4058$  and is shown in the heliocentric rest frame. One (plain line) was observed on HJD 2 452 383.507 (corresponding to  $\phi = 0.78$ , see Table 3) and is exhibiting a RV of  $-48 \text{ km s}^{-1}$ ; the other was observed on HJD 2 453 133.605 ( $\phi = 0.39$ ) corresponding to a velocity of  $-10 \text{ km s}^{-1}$ . The main change between the two spectra is a shift in RV.

We also measured the Ca II  $\lambda 3933$  interstellar absorption line. In the echelle spectra, this line presents at least 5 distinct components. Therefore, we measured the position of the central line of the three main components. Averaging the RVs obtained in the echelle spectra, we derived a mean of  $-30 \pm 4 \text{ km s}^{-1}$ . In Fig. 4 (bottom), we also show the RVs of this Ca II line measured in our WR 25 spectra. This confirms the good agreement existing among the different instrumental configurations used in this work.

Having noticed that the position of the N IV  $\lambda 4058$  line was variable, we studied the time series of the measured RVs. We searched for periodicities using two independent methods: the algorithm to derive periods of cyclic phenomena described in Marraco & Muzzio (1980), and a Fourier-type analysis method by Heck et al. (1985, see also comments by Gosset et al., 2001).

We first analyzed the data set consisting of the 50 high-resolution spectra (HRS). The particular distribution of the observing times induces some aliasing at  $\delta\nu = 0.00045 \text{ d}^{-1}$ , at  $\delta\nu = 0.00270 \text{ d}^{-1}$ , at  $\delta\nu = 0.02540 \text{ d}^{-1}$  and at  $\delta\nu = 0.02810 \text{ d}^{-1}$  as revealed by e.g. the spectral window (see the definition in Deeming, 1975). The Amplitude Spectrum (square root of the power spectrum) of the HRS data is given in Fig. 2. The highest ordinate is located at  $\nu = 0.004795 \text{ d}^{-1}$ . The two neighbouring peaks are aliases of this frequency; this is also the case for the peaks at  $\nu = 0.00209 \text{ d}^{-1}$ , at  $\nu = 0.00749 \text{ d}^{-1}$ , at  $\nu = 0.03015 \text{ d}^{-1}$  and at  $\nu = 0.03286 \text{ d}^{-1}$ . All of them thus belong to the same family and we consider that the dominant frequency is the one at  $\nu = 0.004795 \text{ d}^{-1}$ . This is further confirmed by a decomposition of the RV curve into several frequencies using the multifrequency approach (see Eqs. A11 to A19 in Gosset et al., 2001). The main frequency varies from  $\nu = 0.004795 \text{ d}^{-1}$  to

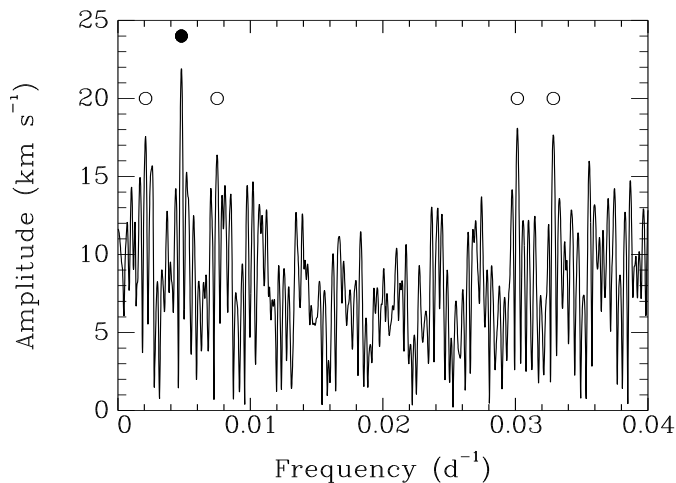


**Fig. 2.** Amplitude Spectrum (square root of the power spectrum) as a function of the frequency expressed in  $\text{d}^{-1}$  and corresponding to the analysis of the HRS data set. From  $0.04 \text{ d}^{-1}$  to  $0.5 \text{ d}^{-1}$ , no peak exceeds  $13 \text{ km s}^{-1}$ . The adopted main frequency is marked by a filled circle and the expected positions of the main aliases of this frequency are marked with open circles.

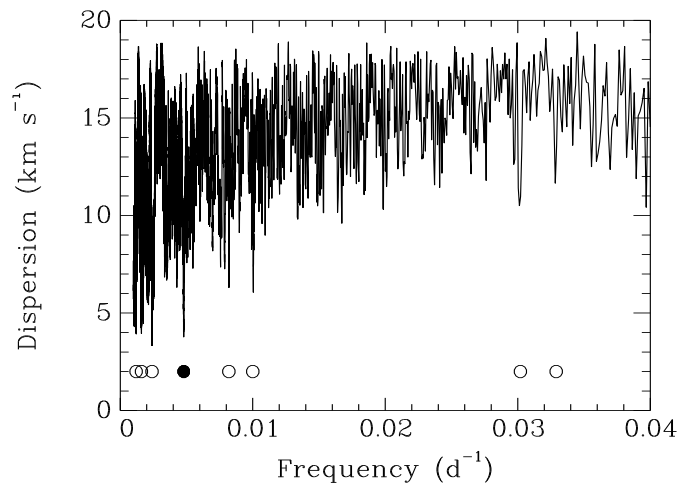


**Fig. 3.** Run of the Marraco & Muzzio (1980) statistic as a function of the frequency expressed in  $\text{d}^{-1}$  and corresponding to the analysis of the HRS data set. The main dips are seen at  $\nu = 0.0012 \text{ d}^{-1}$ ,  $\nu = 0.0016 \text{ d}^{-1}$ ,  $\nu = 0.0024 \text{ d}^{-1}$  and  $\nu = 0.0048 \text{ d}^{-1}$ ; the first three are subharmonics of  $\nu = 0.0048 \text{ d}^{-1}$  and are a well-known artifact of this kind of method. Other dips are visible at  $\nu = 0.0082 \text{ d}^{-1}$ ,  $\nu = 0.0100 \text{ d}^{-1}$ ,  $\nu = 0.0302 \text{ d}^{-1}$  and  $\nu = 0.0329 \text{ d}^{-1}$ . The last two are also aliases of the  $\nu = 0.0048 \text{ d}^{-1}$  dip. The cited frequencies are marked as in Figure 2.

$\nu = 0.004805 \text{ d}^{-1}$  depending on the secondary frequencies being inventoried: we thus adopt  $\nu = 0.00480 \text{ d}^{-1}$  ( $P = 208.3 \text{ d}$ ) as the true progenitor. We estimated the error on the period by taking as a conservative upper limit one tenth of the peak width (which is a function of the time baseline); we derived  $\sigma_\nu = 0.00003 \text{ d}^{-1}$  and thus  $\sigma_P = 1.3 \text{ d}$ . The Marraco & Muzzio method applied to the RVs measured on the HRS spectra gave as a most probable period  $P = 208.3 \pm 0.5 \text{ d}$  along with some aliases, in good agreement with the Fourier results (see Fig. 3).

A phase diagram with the adopted period presents a clear gap (around phase 1.0, see Fig. 4). Therefore, we complemented our HRS data with other data sets. We thus defined two subsequent data sets:

- our 50 RVs measured on the high-resolution spectra (HRS) complemented by the 8 medium-resolution data (MRS) and by the 12 low-resolution spectra (LRS), thus 70 data points labelled HRS+MRS+LRS,
- all our 70 RVs plus the 54 published by Moffat (1978) and Conti et al. (1979), complemented with the RV measured in one spectrum provided by Hamann et al. (1995).

We also ran the period-search algorithms using these enlarged data sets. In the HRS+MRS+LRS data set, the Fourier analysis favoured a frequency  $\nu = 0.004820 \text{ d}^{-1}$  which is within the error bars of the previously quoted one. Finally, the data set all+published indicates a frequency  $\nu = 0.004810 \text{ d}^{-1}$  ( $\sigma_\nu = 7.7 \cdot 10^{-6} \text{ d}^{-1}$ ) corresponding to  $P = 207.9 \text{ d}$  ( $\sigma_P = 0.3 \text{ d}$ ). The Marraco & Muzzio (1980) method applied to the all+published data set similarly gives  $P = 207.8 \pm 0.3 \text{ d}$ .

To further refine the period determination, we ran GBART, an improved version<sup>3</sup> of the orbital solution program originally published by Bertiau & Grobbon (1968), with the three above-mentioned data sets. The RVs measured on HRS were weighted with 1, MRS with 0.5, and LRS or published, with 0.1. The orbital parameters obtained for each data set are explicitly given in Table 3 and the corresponding orbital solutions are depicted in Fig. 4. We obtained quite eccentric orbits with  $e$  ranging between 0.35 and 0.5, orbital semi-amplitudes  $K$  between 33 and  $44 \text{ km s}^{-1}$ , and different values for the orbital period.

The fact that there is no HRS RV more negative than  $-70 \text{ km s}^{-1}$ , while some LRS RVs indicate  $-110 \text{ km s}^{-1}$ , is intriguing. Clearly the HRS data set presents a strong gap around phase 1.0. This gap can be filled by LRS data obtained in May 1973 and April 2001. Even though the errors on these RVs are expected to be larger and despite the low weight given, these LRS data have a large impact on the eccentricity and on the orbital semi-amplitude derived. Adding the published data to ours still yields an orbital solution that remains in good agreement with the HRS+MRS+LRS one. However, none of the published RVs have been acquired near the critical phase (1.0).

Although the exact orbital solution remains uncertain, our various data sets allow us to conclude that WR 25 presents RV variations with a period of about 208 days. These variations are indicative of an eccentric binary system. Strictly periodic RV variations with such a long time-scale are difficult to interpret

<sup>3</sup> Available upon request from <ftp://lilen.fcaglp.unlp.edu.ar/pub/fede/gbart-0.1-41.tar.gz>

**Table 3.** Orbital solutions corresponding to the RVs of the N IV  $\lambda 4058$  emission line within different data sets. The quoted errors correspond to  $1\sigma$  uncertainties. Symbols have the canonical meaning. The last three correspond, respectively, to the mass function, the standard deviation of the fit and the number of data points involved.

	HRS only	HRS+MRS+LRS	All + published
$P$ [d]	$208.3 \pm 0.2$	$207.9 \pm 0.1$	$207.85 \pm 0.02$
$V_0$ [km s $^{-1}$ ]	$-30.6 \pm 0.7$	$-34.2 \pm 0.7$	$-34.6 \pm 0.5$
$K$ [km s $^{-1}$ ]	$33 \pm 2$	$42 \pm 2$	$44 \pm 2$
$e$	$0.35 \pm 0.03$	$0.48 \pm 0.02$	$0.50 \pm 0.02$
$\omega$ [degrees]	$227 \pm 4$	$216 \pm 3$	$215 \pm 3$
$T_{\text{Periastr}}$ [d]*	$1598 \pm 3$	$1597 \pm 2$	$1598 \pm 1$
$T_{\text{RVmax}}$ [d]*	$1654 \pm 3$	$1655 \pm 2$	$1654 \pm 1$
$a \sin i$ [ $R_{\odot}$ ]	$125 \pm 8$	$151 \pm 9$	$156 \pm 8$
$F(\mathcal{M})$ [ $M_{\odot}$ ]	$0.6 \pm 0.1$	$1.1 \pm 0.2$	$1.2 \pm 0.2$
$\sigma$ [km s $^{-1}$ ]	2.5	3.7	4.7
$n$	50	70	124

\*: Heliocentric Julian Date 2,450,000+

in other terms. The exact values for some of the parameters are highly dependent on low resolution data. Therefore, we need further good quality high-resolution data in order to derive a fully definitive orbital solution for the WR primary.

We also considered other lines in the HRS spectra of WR 25. Clearly, certain lines such as N v  $\lambda\lambda 4603\text{-}4619$  vary in agreement with the derived orbital solutions. However, some absorption lines such as He I  $\lambda 5876$  and  $\lambda 4471$  seem to vary in anti-phase, plausibly revealing the signature of the binary companion.

Studying other lines will help to verify whether the RVs derived from the motion of N IV  $\lambda 4058$  represent the orbital motion of the primary; this can not be established on the basis of a single line. This is beyond the scope of the present paper and requires high-resolution high S/N data covering all the phases.

#### 4. Conclusions

We have found that the RVs of the N IV  $\lambda 4058$  emission line in the spectrum of WR 25 show variations with a period of about  $P=208$  days. These variations indicate that the WN star WR 25 is an eccentric binary system.

The He I  $\lambda 5876$  and  $\lambda 4471$  absorption lines seem to show an anti-phase motion and should thus partly belong to the companion which is supposed to be of the OB type.

The companion seems to be fainter than the WR primary, indicating that WR 25 is perhaps another example of a young binary system where the WR component is the most massive star. The prototype of this class is WR 22 (WN7h+O9III-V, van der Hucht, 2001) which turned out to be a massive binary system ( $55 M_{\odot} + 21 M_{\odot}$ ) in an 80-day period orbit (Rauw et al., 1996; Schweickhardt et al., 1999). The primary of WR 22 is most probably an example of the long-searched for case of a core H burning star resembling a WR star due to its luminosity and mass. The star is on its way to becoming a hydrogen-free

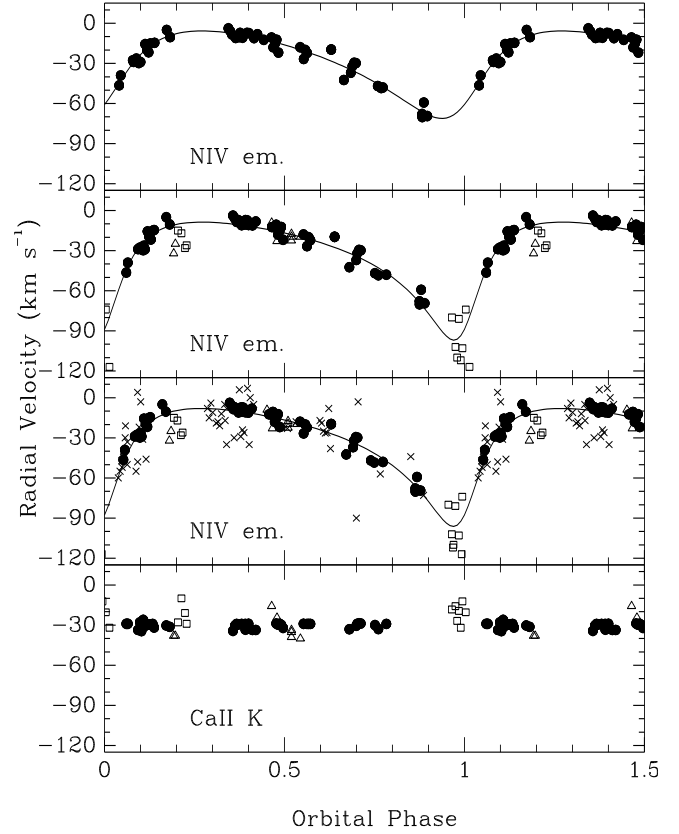


**Fig. 4.** Observed radial velocities (along with the fitted models) corresponding to the N IV  $\lambda 4058$  emission line in the spectra of WR 25. The data are phased according to the ephemeris as given in Table 3; phase 0.0 corresponds to periastron. The different panels illustrate different analyzed data sets. *Top*: Our HRS data only (filled circles). *Middle top*: HRS+MRS+LRS data; open triangles represent the RVs in the MRS set, and squares the LRS ones. *Middle bottom*: All + published data; crosses are the RVs from Conti et al. (1979), Moffat (1978), and Hamann et al. (1995). In each plot, the solid curve represents the relevant orbital solution as given in Table 3. *Bottom*: Radial velocities of the interstellar Ca II K absorption feature measured on our spectra.

WR-type star. These objects are extremely rare and thus interesting to study in detail.

WR 25 is one of the brightest WN stars in the X-ray domain, too bright to be explained by intrinsic X-ray emission. It thus was customarily classified as a putative colliding-wind binary. Fig. 4 is the first proof that WR 25 is a binary as suspected from its X-ray emission. On the basis of the existing *XMM-Newton* data, Pollock & Corcoran (2006) found that the X-ray emission of WR 25 is variable although the period cannot be derived independently from the X-ray data alone. WR 25 was brighter in the X-ray domain on JD 2452 842.6 which according to our ephemeris corresponds to a phase of 0.96-0.98. The star thus seems to be brighter at periastron as predicted for colliding-wind binaries in the adiabatic regime (see e.g. Stevens et al., 1992). Although this should be further investi-

gated, WR 25 appears to be an example of a colliding-wind binary system.

We are currently planning to monitor the optical spectrum of WR 25 around the expected time of minimum radial velocity of the WR emission lines in order to derive a full definitive orbital solution. High-resolution high S/N ratio data are essential. These spectra will help to improve the orbital solution, and to detect the absorption lines of the companion, which for this particular phase domain should be located to the red of the WN emission line, thus avoiding confusion with the absorption components of P-Cygni profiles from the primary.

*Acknowledgements.* The Liège team is greatly indebted to the Fonds National de la Recherche Scientifique (FNRS, Belgium) for support. This research is supported in part by contract P5/36 IAP (Belspo) and through the PRODEX XMM and INTEGRAL contracts. The La Plata team thanks the Directors and staff of CASLEO, LCO, and CTIO for the use of their facilities, and acknowledges the use, at CASLEO, of the CCD and data acquisition system supported under US NSF grant AST-90-15827 to R.M. Rich. We also thank Nolan Walborn for his useful comments on this work, and Mariela Corti for kindly obtaining 3 spectra for us. RB acknowledges the support of FONDECYT Program No 1050052. This research has also received partial financial support from IALP, CONICET, Argentina.

## References

- Berghöfer, T. W., Schmitt, J. H. M. M., Danner, R., & Cassinelli, J. P. 1997, *A&A*, 322, 167
- Bertiau, F. & Grobben, J. 1968, *Ric. Astr. Spec. Vat.*, 8, 1
- Conti, P. S., Leep, E. M., & Lorre, J. J. 1977, *ApJ*, 214, 759
- Conti, P. S., Niemela, V. S., & Walborn, N. R. 1979, *ApJ*, 228, 206
- Deeming, T. J. 1975, *Ap&SS*, 36, 137
- Drissen, L., Robert, C., & Moffat, A. F. J. 1992, *ApJ*, 386, 288
- Gosset, E., Royer, P., Rauw, G., Manfroid, J., & Vreux, J.-M. 2001, *MNRAS*, 327, 435
- Gosset, E., Nazé, Y., Claeskens, J.-F., et al. 2005, *A&A*, 429, 685
- Hamann, W.-R., Koesterke, L., & Wessolowski, U. 1995, *A&AS*, 113, 459
- Heck, A., Manfroid, J., & Mersch, G. 1985, *A&AS*, 59, 63
- Marraco, H. G. & Muzzio, J. C. 1980, *PASP*, 92, 700
- Meynet, G. & Maeder, A. 2005, *A&A*, 429, 581
- Moffat, A. F. J. 1978, *A&A*, 68, 41
- Niemela, V. S., 1973, *PASP*, 85, 220
- Oskinova, L. M., Ignace, R., Hamann, W.-R., Pollock, A. M. T., & Brown, J. C. 2003, *A&A*, 402, 755
- Pollock, A. M. T. 1991, in *IAU Symp. 143: Wolf-Rayet Stars and Interrelations with Other Massive Stars in Galaxies*, eds. K. A. van der Hucht & B. Hidayat, Dordrecht: Kluwer Ac. Publ., p.105
- Pollock, A. M. T. & Corcoran, M. F. 2006, *A&A*, 445, 1093
- Raassen, A. J. J., van der Hucht, K. A., Mewe, R., et al. 2003, *A&A*, 402, 653
- Rauw, G., Vreux, J.-M., Gosset, E., et al. 1996, *A&A*, 306, 771
- Sana, H., Rauw, G., Nazé, Y., Gosset, E., & Vreux, J.-M. 2006, *MNRAS*, in press
- Schweickhardt, J., Schmutz, W., Stahl, O., Szeifert, T., & Wolf, B. 1999, *A&A*, 347, 127
- Seward, F. D. & Chlebowski, T. 1982, *ApJ*, 256, 530
- Smith, L. F. 1968, *MNRAS*, 138, 109
- Smith, L. F., Shara, M. M., & Moffat, A. F. J. 1996, *MNRAS*, 281, 163
- Stevens, I. R., Blondin, J. M., & Pollock, A. M. T. 1992, *ApJ*, 386, 265
- van der Hucht, K. A., Conti, P. S., Lundström, I., & Stenholm, B. 1981, *Space Sci.Rev.*, 28, 227
- van der Hucht, K. A. 2001, *New Astronomy Review*, 45, 135
- Walborn, N. R. 1974, *ApJ*, 189, 269
- Walborn, N. R. & Fitzpatrick, E. L. 2000, *PASP*, 112, 50

## List of Objects

‘HD 93162’ on page 1

‘HD 92740’ on page 2

‘HD 93131’ on page 2

<sup>1</sup> Departamento de Física, Universidad de La Serena, Benavente 980, La Serena, Chile

e-mail: rgamen@dfu1s.cl

<sup>2</sup> Institut d’Astrophysique et de Géophysique, Université de Liège, Allée du 6 Août, 17, B-4000, Liège (Sart Tilman), Belgium

e-mail: gosset@astro.ulg.ac.be

<sup>3</sup> Las Campanas Observatory, The Carnegie Observatories, Casilla 601, La Serena, Chile

e-mail: nmorrell@lco.cl

<sup>4</sup> Facultad de Ciencias Astronómicas y Geofísicas, Universidad de La Plata, Paseo del Bosque S/N, 1900, La Plata, Argentina

e-mail: virpi@fcaglp.unlp.edu.ar

<sup>5</sup> European Southern Observatory, Casilla 19001, Santiago 19, Chile

e-mail: hsana@eso.org